Research Article

INTERNATIONAL JOURNAL OF ADVANCED ROBOTIC SYSTEMS

International Journal of Advanced Robotic Systems
January-February 2017: 1–12

DOI: 10.1177/1729881416687127
journals.sagepub.com/home/arx
SAGE

Passive impedance-based second-order sliding mode control for non-linear teleoperators

Luis G García-Valdovinos[1], Hugo Santacruz-Reyes[1], Alan G López-Segovia[1], Manuel Bandala-Sánchez[1] and Luis A García-Zarco[2]

Abstract

Bilateral teleoperation systems have attracted significant attention in the last decade mainly because of technological advancements in both the communication channel and computers performance. In addition, non-linear multi-degree-of-freedom bilateral teleoperators along with state observers have become an open research area. In this article, a model-free exact differentiator is used to estimate the full state along with a chattering-free second-order sliding mode controller to guarantee a robust impedance tracking under both constant and an unknown time delay of non-linear multi-degree-of-freedom robots. The robustness of the proposed controller is improved by introducing a change of coordinates in terms of a new nominal reference similar to that used in adaptive control theory. Experimental results that validate the predicted behaviour are presented and discussed using a Phantom Premium 1.0 as the master robot and a Catalyst-5 virtual model as the slave robot. The dynamics of the Catalyst-5 system is solved online.

Keywords

Bilateral teleoperation, impedance control, exact differentiator, higher-order sliding mode control, constant time delay

Date received: 13 March 2016; accepted: 23 November 2016

Topic: Robot Manipulation and Control
Topic Editor: Andrey V Savkin
Associate Editor: Istvan Harmati

Introduction

Most teleoperation schemes that consider (constant or varying) time delays (induced by the communication channel) have been proposed in the last decade for non-linear multi-degree-of-freedom (DOF) manipulators; for instance, the studies discussed in the literature.[1–4] Outstanding complete surveys on bilateral teleoperation schemes are the studies discussed in the literature.[5–8]

Many of the published works have addressed the problem of controlling a teleoperation system assuming that velocity can be measurable; however, in practice, velocity (even acceleration) is hardly available. There are few remarkable exceptions addressing this problem.[9–12]A model-free sliding mode-based observer (achieving finite-time convergence of the estimation error) is implemented in the study by Garcia-Valdovinos et al.[9] The work discussed by Garcia-Valdovinos et al.[10] is the first formal work addressing the use of velocity and acceleration observers for bilateral

[1] Center for Engineering and Industrial Development, Santiago de Querétaro, Querétaro, México
[2] Lazaro Cardenas Institute of Technology, Lázaro Cárdenas City, Michoacán, México

Corresponding author:
Luis G García-Valdovinos, Center for Engineering and Industrial Development, Avenida Playa Pie de la Cuesta 702, Desarrollo San Pablo, Querétaro 76130, México.
Email: ggarcia@cidesi.edu.mx

teleoperators. A variable structure controller coupled with an adaptive perturbation estimation is proposed in the study by Ghafarirad et al.[11] for trajectory tracking of position using a piezoelectric device. A super-twisting observer is proposed in the study by Gonzalez et al.[12] to estimate velocity and acceleration in non-linear bilateral teleoperators.

Regarding sliding mode control, Buttolo et al.[13] proposed model-based first-order sliding mode controllers for both master and slave stations, achieving an improvement with respect to position tracking and parametric uncertainty. Although a good level of transparency is achieved, the inherent effects of the first-order sliding mode control due to the high-frequency signals of the control input make it unsuitable to be implemented in a physical system, leading to an unexpectedly deterioration of the overall system performance and, therefore, loss of transparency. Park and Cho[14] proposed to implement an impedance control for the master and a modified first-order sliding mode control for the slave, in which the gain that satisfies the sliding condition can be set independently of time delays. Thus, this scheme results to be robust against a constant time delay. Nevertheless, this scheme easily becomes unstable when interacting with rigid environments. To deal with this issue, the same authors proposed a sliding mode impedance control for the slave in order to reduce the impact forces and achieve a sustained stable contact.[15] Similarly, in the study by Cho and Park,[16] the problem of parametric uncertainty is studied. Additionally, an algorithm for parameter tuning is provided. However, the signum function used for the sliding mode is replaced by a saturation function to reduce the chattering, resulting in poor tracking performance, hence, a low degree of transparency. A number of bilateral teleoperation schemes addressing first-order sliding mode controls, most of them model-based schemes, have been published in recent years, for instance,[11,17,18,19,20] where some sort of state estimation has been used.

Finally, the literatures[9,10,12,21,22] proposed modified schemes based on higher-order sliding modes to avoid the addition of chattering to the system. Formal and rigorous stability proofs, taking into account state observers for both master and slave robots, are considered for linear and non-linear systems.

In this article, a new nominal reference is proposed in order to introduce a change of coordinates into the slave closed-loop dynamics. The approach yields significant improvement of the robustness of the system along with the chattering-free second-order sliding mode control. The slave control scheme withstands parametric uncertainty and guarantees exponential tracking position with an acceptable sustained contact force tracking, under an unknown constant time delay. An exact differentiator, proposed in the study by Levant,[23] is implemented to estimate robust velocity and acceleration, without previous knowledge of any system parameters.

The proposed scheme is developed for non-linear systems, and a formal analysis of stability is presented. Experimental results validate the proposed bilateral teleoperation scheme.

Dynamics of the teleoperation system

Both the master and the slave manipulators are modelled as a pair of non-linear (n)-DOFs serial links with revolute joints, as follows

$$\mathbf{H}_m(\mathbf{q}_m)\ddot{\mathbf{q}}_m + \mathbf{C}_m(\mathbf{q}_m, \dot{\mathbf{q}}_m)\dot{\mathbf{q}}_m + \mathbf{g}_m(\mathbf{q}_m) = \boldsymbol{\tau}_m + \boldsymbol{\tau}_h \quad (1)$$

$$\mathbf{H}_s(\mathbf{q}_s)\ddot{\mathbf{q}}_s + \mathbf{C}_s(\mathbf{q_s}, \dot{\mathbf{q}}_s)\dot{\mathbf{q}}_s + \mathbf{g}_s(\mathbf{q}_s) = \boldsymbol{\tau}_s - \boldsymbol{\tau}_e \quad (2)$$

where $\mathbf{q}_i,\ \dot{\mathbf{q}}_i,\ \ddot{\mathbf{q}}_i \in \mathbb{R}^n$ are the position, velocity, and joint acceleration, respectively; $\mathbf{H}_i(\mathbf{q}_i) \in \mathbb{R}^{n\times n}$ are the inertia matrices; $\mathbf{C}_i(\mathbf{q}_i, \dot{\mathbf{q}}_i) \in \mathbb{R}^{n\times n}$ are the Coriolis and centripetal forces; $\mathbf{g}_i(\mathbf{q}_i) \in \mathbb{R}^n$ denote the gravitational torques; $\boldsymbol{\tau}_i \in \mathbb{R}^n$ are the control inputs; and $\boldsymbol{\tau}_h \in \mathbb{R}^n$ and $\boldsymbol{\tau}_e \in \mathbb{R}^n$ represent, respectively, the torque exerted by the human operator and the environment interaction. Here $i = \mathrm{m}$ represents the master robot and $i = \mathrm{s}$ the slave robot.

Impedance control technique

The impedance control technique proposed by Hogan[24] is one of the fundamental approaches for force tracking control in robot manipulators with constrained motion. Impedance control regulates the force between a manipulator and the environment by defining the target impedance relationship between position and contact force. The desired force is indirectly controlled by pre-specifying a robot positional reference trajectory that is determined based on the stiffness and environment location.

Typically, the task is defined in the Cartesian space and hence, an accepted choice is to design the target impedance for each teleoperator in the same space. To this end, joint dynamics (1) and (2) have to be transformed into the Cartesian dynamics by means of the forward and differential kinematics as follows (from this point forward, without loss of generality, arguments are omitted for simplicity)

$$\mathbf{H}_m(\mathbf{x}_m)\ddot{\mathbf{x}}_m + \mathbf{C}_m(\mathbf{x}_m, \dot{\mathbf{x}}_m)\dot{\mathbf{x}}_m + \mathbf{G}_m = \mathbf{F}_m + \mathbf{F}_h \quad (3)$$

$$\mathbf{H}_s(\mathbf{x}_s)\ddot{\mathbf{x}}_s + \mathbf{C}_s(\mathbf{x}_s, \dot{\mathbf{x}}_s)\dot{\mathbf{x}}_s + \mathbf{G}_s = \mathbf{F}_s - \mathbf{F}_e \quad (4)$$

where expressions for the master ($i = m$) and the slave ($i = s$) are as follows

$$\begin{aligned} \mathbf{H}_i(\mathbf{x}_i) &= \mathbf{J}_i^{-T}\mathbf{H}_i\mathbf{J}_i^{-1} \\ \mathbf{C}_i(\mathbf{x}_i, \dot{\mathbf{x}}_i) &= \mathbf{J}_i^{-T}\mathbf{C}_i\mathbf{J}_i^{-1} - \mathbf{J}_i^{-T}\mathbf{H}_i\mathbf{J}_i^{-1}\dot{\mathbf{J}}_i\mathbf{J}_i^{-1} \\ \mathbf{G}_i &= \mathbf{J}_i^{-T}\mathbf{g}_i \end{aligned} \quad (5)$$

where $\mathbf{x}_i \in \mathbb{R}^n$ is the end-effector position and orientation, $\mathbf{H}_i \in \mathbb{R}^{n\times n}$ are the Cartesian inertia matrices, $\mathbf{C}_i \in \mathbb{R}^{n\times n}$ are the Coriolis and centripetal forces, $\mathbf{G}_i \in \mathbb{R}^n$ denote the gravitational forces, $\mathbf{F}_m = \mathbf{J}_m^{-\mathrm{T}}\boldsymbol{\tau}_m$ and $\mathbf{F}_s = \mathbf{J}_s^{-\mathrm{T}}\boldsymbol{\tau}_s$, are the Cartesian controllers for both master and slave robots, respectively, $\mathbf{J}_i^{-\mathrm{T}} \in \mathbb{R}^{n\times n}$ represent the transpose inverse Jacobians, and $\mathbf{F}_h \in \mathbb{R}^n$ and $\mathbf{F}_e \in \mathbb{R}^n$ represent the force exerted by the human operator and the environment interaction, respectively, which in practice are measured by force sensors.

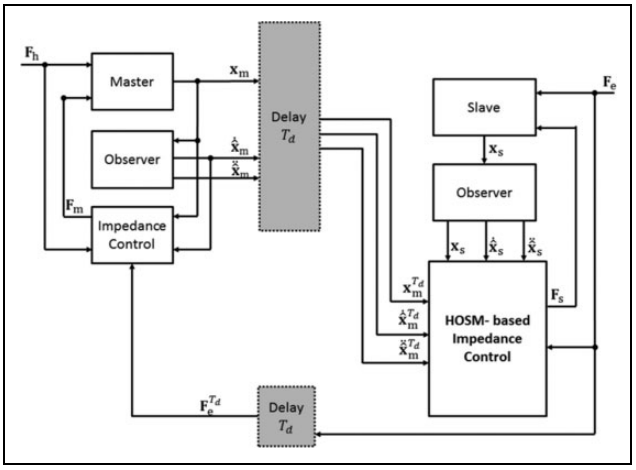

Figure 1. Block diagram of the proposed bilateral teleoperation scheme.

Delayed signals and scale factors

Prior to defining the controller design, it is necessary to define the variables exchanged between each site. Variables sent from the master to the slave are

$$\begin{aligned}\mathbf{x}_m^{T_d}(t) &= \mathbf{x}_m(t-T_d)\\ \dot{\mathbf{x}}_m^{T_d}(t) &= \dot{\mathbf{x}}_m(t-T_d)\\ \ddot{\mathbf{x}}_m^{T_d}(t) &= \ddot{\mathbf{x}}_m(t-T_d)\end{aligned} \tag{6}$$

where T_d denotes the constant time delay induced by the communication channel. To simplify the notation, time delay is the same in both directions, from master to slave and vice versa. The only variable sent from the slave to the master is the environment force

$$\mathbf{F}_e^{T_d}(t) = \mathbf{F}_e(t-T_d) \tag{7}$$

Figure 1 shows the information that is exchanged between the master station and the slave station.

Position, velocity, and acceleration of the master as well as the environment contact force of the slave can be scaled up or down by means of the diagonal matrices $\mathbf{K}_p$ and $\mathbf{K}_f$, depending on the task to be performed. At this point, the problem is to design $\mathbf{F}_m$ and $\mathbf{F}_s$ subject to unmeasurable $\ddot{\mathbf{x}}_m$, $\ddot{\mathbf{x}}_s$, $\dot{\mathbf{x}}_m$, $\dot{\mathbf{x}}_s$ and a number of uncertain robot parameters, such that slave position, velocity, and acceleration asymptotically converge to the scaled master position, velocity, and acceleration, respectively, as time goes by

$$\begin{aligned}\mathbf{x}_s(t) &\to \mathbf{K}_p\mathbf{x}_m^{T_d}(t)\\ \dot{\mathbf{x}}_s(t) &\to \mathbf{K}_p\dot{\mathbf{x}}_m^{T_d}(t)\\ \ddot{\mathbf{x}}_s(t) &\to \mathbf{K}_p\ddot{\mathbf{x}}_m^{T_d}(t)\end{aligned} \tag{8}$$

with kinesthetic perception of $\mathbf{K}_f\mathbf{F}_e^{T_d}$ at the master side. In the next section, a model-free exact differentiator[23] is proposed to estimate in finite time, the Cartesian velocity and acceleration of both master and slave teleoperators.

Remark 1. Matrices $\mathbf{K}_p$ and $\mathbf{K}_f$ suggest the use of a different scaling factor value for each coordinate (x, y, z); however, for simplicity, a unique scaling factor will be considered here. Let us consider the new notation for position scaling

$$\begin{aligned}\mathbf{x}_s(t) &\to \mathrm{k}_p\mathbf{x}_m^{T_d}(t)\\ \dot{\mathbf{x}}_s(t) &\to \mathrm{k}_p\dot{\mathbf{x}}_m^{T_d}(t)\\ \ddot{\mathbf{x}}_s(t) &\to \mathrm{k}_p\ddot{\mathbf{x}}_m^{T_d}(t)\end{aligned} \tag{9}$$

and for force scaling

$$k_f\mathbf{F}_e^{T_d} \tag{10}$$

where k_p and k_f are positive scalars and denote the scaling factors.

Velocity and acceleration observer

Real-time access to the states, particularly velocity and acceleration, has always been a challenging problem. Either the dirty-Euler differentiator, along with a filter technique, or observers (whether these are linear or nonlinear, model-based or model-free) are good options to deal with the lack of velocity and/or acceleration sensors. In 2003, Levant[23] proposed an arbitrary-order real-time differentiator that allows robust exact differentiation up to any given order l provided the next $(l+1)$th derivative is bounded by a known constant. In this work, velocity and acceleration signals of the master and the slave robots are obtained by means of the exact differentiator, preserving the stability of the system and achieving an adequate performance in comparison to the typical Euler differentiator. In our case, $l = 2$ means that the measured position $\mathbf{x}_i = [\,x_i \quad y_i \quad z_i\,]$, with $i = \{m, s\}$, is differentiated twice. For instance, let us consider the following differentiator for the master position in the x-axis

$$\begin{aligned}\dot{w}_0 &= -\lambda_0|w_0 - x_m|^{\frac{2}{3}}\operatorname{sign}(w_0 - x_m) + w_1\\ \dot{w}_1 &= -\lambda_1|w_1 - \dot{w}_0|^{\frac{1}{2}}\operatorname{sign}(w_1 - \dot{w}_0) + w_2\\ \dot{w}_2 &= -\lambda_2\operatorname{sign}(w_2 - \dot{w}_1)\end{aligned} \tag{11}$$

where $\lambda_0, \lambda_1, \lambda_2 > 0$ are observer's constants. In the same fashion, an exact differentiator can be designed for each of the $\mathbf{x}_i$ components of the respective teleoperator, that is, a total of six differentiators (observers) have to be implemented, three for the master and three for the slave, and one for each x_i, y_i, and z_i component. After solving system (11), $\hat{x}_m = w_0$, $\dot{\hat{x}}_m = w_1$, and $\ddot{\hat{x}}_m = w_2$ are, respectively, the estimated position, velocity, and acceleration in the x-axis of the master. The same applies for the remaining components. Note that, in general, a different set of constant gains $\lambda_0, \lambda_1, \lambda_2$ has to be tuned for each differentiator; see the study by Levant[23] for major details.

Master controller design

Commonly when driving a master robot, it is expected that the human operator feels very low friction and inertia. However, in some cases, it is preferable, even convenient, for the human operator to choose arbitrarily a comfortable damping/inertia by tuning some parameters. The latter is possible if a desired impedance dynamics is imposed on the master robot, as follows

$$\bar{\mathbf{M}}_m\ddot{\mathbf{x}}_m + \bar{\mathbf{B}}_m\dot{\mathbf{x}}_m + \bar{\mathbf{K}}_m\mathbf{x}_m = \mathbf{F}_h - \mathrm{k}_f\mathbf{F}_e^{T_d} \tag{12}$$

where $\bar{\mathbf{M}}_m$, $\bar{\mathbf{B}}_m$, $\bar{\mathbf{K}}_m$ are $n\times n$ diagonal positive definite matrices denoting, respectively, desired inertia, damping, and stiffness. Thus, the master controller, which guarantees the desired impedance dynamics (12), is designed as follows.

Solving for $\mathbf{F}_m$ in equation (3), we obtain

$$\mathbf{F}_m = \mathbf{H}_m\ddot{\mathbf{x}}_m + \mathbf{C}_m\dot{\mathbf{x}}_m + \mathbf{G}_m - \mathbf{F}_h \tag{13}$$

Now, solving for $\ddot{\mathbf{x}}_{\mathrm{m}}$ in equation (12) and substituting into equation (13) result the control law for the master

$$\begin{aligned}\mathbf{F}_m = \mathbf{H}_m\bar{\mathbf{M}}_m^{-1}[\mathbf{F}_h - \mathrm{k}_f\mathbf{F}_e^{T_d} - \bar{\mathbf{B}}_m\dot{\hat{\mathbf{x}}}_m - \bar{\mathbf{K}}_m\mathbf{x}_m] \\ +\mathbf{C}_m\dot{\hat{\mathbf{x}}}_m + \mathbf{G}_m - \mathbf{F}_h\end{aligned} \tag{14}$$

From equation (14), note that the master velocity and acceleration have been replaced by their estimate velocity and acceleration given by the observer (11). Since estimation errors exhibit finite-time convergence, thus, equation (12) will arise.

The master impedance control law (14) enforces the desired impedance (12) in closed loop, whose parameters are chosen by the user depending on a specific task, such that[22]:

If the slave robot *does not touch* the environment, $\mathbf{F}_e^{T_d} = 0$. Then equation (12) becomes a mass-spring-damper system driven solely by the human force $\mathbf{F}_h$. Note that, in this case, the controller is in *impedance position mode*.

If the slave robot *does touch* the environment, $\mathbf{F}_e^{T_d} > 0$. Then equation (12) becomes a mass-spring-damper system driven by force error $\mathbf{F}_h - \mathrm{k}_f\mathbf{F}_e^{T_d}$. In this case, the actuators in the master station make the human to perceive a *scaled contact force* equal to $k_f\mathbf{F}_e^{T_d}$. Note that, when the slave is in contact, the master control is in *force control mode*. In this mode, the human could virtually recreate, cognitively, the surface of the object that the slave is touching according to this vector, through kinesthetic sensations and the visual information also coming from the slave station.

Remark 2. The master Cartesian control law can be mapped into joint control law multiplying equation (13) by the transpose of the master Jacobian, as shown below

$$\boldsymbol{\tau}_m = \mathbf{J}_m^T\mathbf{F}_m \tag{15}$$

Next, the design of the slave controller is given.

Slave controller design

Under similar rationale on the master controller design, we now introduce a change of coordinates in order to tailor an extended error variable to induce a second-order sliding mode and, thus, to produce a desired impedance behaviour modulated by the environmental contact force. Remember that this controller must withstand constant time delay. To this end, the desired slave impedance model becomes now the desired manifold to converge. In other words, we need to design a controller to guarantee that the closed-loop error equation yields the desired slave impedance model. That is, the controller must satisfy the sliding condition at the desired slave impedance model.

Desired slave impedance model

The desired impedance characteristic for the slave robot is defined as follows

$$\bar{\mathbf{M}}_s\ddot{\tilde{\mathbf{x}}}_s + \bar{\mathbf{B}}_s\dot{\tilde{\mathbf{x}}}_s + \bar{\mathbf{K}}_s\tilde{\mathbf{x}}_s = -\mathbf{F}_e \tag{16}$$

where $\bar{\mathbf{M}}_s$, $\bar{\mathbf{B}}_s$, $\bar{\mathbf{K}}_s$ are $n \times n$ diagonal positive definite matrices, denoting desired inertia, damping, and stiffness, respectively, and the slave tracking errors are $\ddot{\tilde{\mathbf{x}}}_s = \ddot{\hat{\mathbf{x}}}_s - k_p\ddot{\mathbf{x}}_m^{T_d}$, $\dot{\tilde{\mathbf{x}}}_s = \dot{\hat{\mathbf{x}}}_s - k_p\dot{\mathbf{x}}_m^{T_d}$ and $\tilde{\mathbf{x}}_s = \mathbf{x}_s - k_p\mathbf{x}_m^{T_d}$ for acceleration, velocity, and position, respectively. Since the objective is to achieve the impedance error model (16) in closed loop, then naturally the sliding surface is, from equation (16)

$$\hat{\mathbf{I}}_e(t) = \bar{\mathbf{M}}_s\ddot{\tilde{\mathbf{x}}}_s + \bar{\mathbf{B}}_s\dot{\tilde{\mathbf{x}}}_s + \bar{\mathbf{K}}_s\tilde{\mathbf{x}}_s + \mathbf{F}_e = 0 \tag{17}$$

A dynamic change of coordinates

Let us consider the following nominal reference in order to introduce a change of coordinates in the closed-loop system

$$\begin{aligned}\dot{\hat{\mathbf{x}}}_r = \mathrm{k}_p\dot{\mathbf{x}}_m^{T_d} - \bar{\mathbf{M}}_s^{-1}\left[\bar{\mathbf{B}}_s\tilde{\mathbf{x}}s + \int_0^t F(t)\,\mathrm{d}t\right] \\ -\bar{\mathbf{M}}_s^{-1}\mathbf{K}_i\int_0^t\int_{\mathrm{o}}^t \mathrm{sign}\left(\hat{\mathbf{I}}_q(t)\right)\mathrm{d}t\,\mathrm{d}t\end{aligned} \tag{18}$$

where $(t) = \bar{\mathbf{K}}_s\tilde{\mathbf{x}}_s(t) + \mathbf{F}_e(t) - \hat{\mathbf{I}}_{ep}(t_0)\,\mathrm{e}^{-\kappa t}$, and with its time derivative

$$\begin{aligned}\ddot{\hat{\mathbf{x}}}_r = \mathrm{k}_p\ddot{\mathbf{x}}_m^{T_d} - \bar{\mathbf{M}}_s^{-1}\left[\bar{\mathbf{B}}_s\dot{\tilde{\mathbf{x}}}_s + \mathbf{F}(t)\right] \\ -\bar{\mathbf{M}}_s^{-1}\mathbf{K}_i\int_0^t \mathrm{sign}\left(\hat{\mathbf{I}}_q(t)\right)\mathrm{d}t\end{aligned} \tag{19}$$

where $\hat{\mathbf{I}}_{ep} = \bar{\mathbf{M}}_s\ddot{\tilde{\mathbf{x}}}_s + \bar{\mathbf{B}}_s\dot{\tilde{\mathbf{x}}}_s + \bar{\mathbf{K}}_s\tilde{\mathbf{x}}_s$ evaluated at $t_0 = (t = 0)$ is used to enforce the sliding mode at $t = 0$, as it will be seen afterwards, and $\hat{\mathbf{I}}_q(t) = \hat{\mathbf{I}}_e(t) - \hat{\mathbf{I}}_{ep}(t_0)e^{-\kappa t}$.

Note that, $\hat{\mathbf{I}}_{ep}(t_0)e^{-\kappa t}$ is a vanishing function that has been introduced to enforce the sliding mode condition since the beginning; that is, to remove the reaching phase by bending the sliding surface $\hat{\mathbf{I}}_e(t)$ such that the state of the closed-loop dynamics belongs to the bent hyperplane $\hat{\mathbf{I}}_q(t_0) = 0$, at any given initial condition.

Open-loop error dynamics

Equation (4) is linearly parameterizable[25] by the product of a regressor $\mathbf{Y} = \mathbf{Y}(\mathbf{x}, \dot{\mathbf{x}}, \ddot{\mathbf{x}}) \in \mathbb{R}^{n\times p}$. The regressor is composed of known non-linear functions and a vector $\boldsymbol{\Theta} \in \mathbb{R}^p$, which represents lumped constant parameters. Therefore, the parameterization $\mathbf{Y}\boldsymbol{\Theta}$ can be written in terms of the nominal reference (18) and its derivative (19), as follows

$$\mathbf{H}_s\ddot{\hat{\mathbf{x}}}_r + \mathbf{C}_s\dot{\hat{\mathbf{x}}}_r + \mathbf{G}_s = \hat{\mathbf{Y}}_r\boldsymbol{\Theta} \tag{20}$$

where the regressor $\hat{\mathbf{Y}}_r = \hat{\mathbf{Y}}_r(\mathbf{x}, \dot{\mathbf{x}}, \dot{\hat{\mathbf{x}}}_r, \ddot{\hat{\mathbf{x}}}_r) \in \mathbb{R}^{n\times p}$. Subtracting equation (20) in both sides of equation (4) yields the open-loop error dynamics in terms of the extended error variable $\hat{\boldsymbol{\Omega}}_r$, as follows

$$\begin{aligned}\mathbf{H}_s(\ddot{\mathbf{x}}_s - \ddot{\hat{\mathbf{x}}}_r) + \mathbf{C}_s(\dot{\mathbf{x}}_s - \dot{\hat{\mathbf{x}}}_r) &= \mathbf{F}_s - \mathbf{F}_e - \hat{\mathbf{Y}}_r\boldsymbol{\Theta}\\ \mathbf{H}_s\dot{\hat{\boldsymbol{\Omega}}}_r + \mathbf{C}_s\hat{\boldsymbol{\Omega}}_r &= \mathbf{F}_s - \mathbf{F}_e - \hat{\mathbf{Y}}_r\boldsymbol{\Theta}\end{aligned} \tag{21}$$

with $\hat{\boldsymbol{\Omega}}_r = \dot{\mathbf{x}}_s - \dot{\hat{\mathbf{x}}}_r$ defined as

$$\begin{aligned}\hat{\boldsymbol{\Omega}}_r = {} & \dot{\tilde{\mathbf{x}}}_s + \bar{\mathbf{M}}_s^{-1}\left[\bar{\mathbf{B}}_s\tilde{\mathbf{x}}_s + \int_0^t \mathbf{F}(t)\,\mathrm{d}t\right]\\ & + \bar{\mathbf{M}}_s^{-1}\mathbf{K}_i\int_0^t\int_o^t \operatorname{sign}\left(\hat{\mathbf{I}}_q(t)\right)\mathrm{d}t\,\mathrm{d}t\\ = {} & \bar{\mathbf{M}}_s^{-1}\left[\int_0^t \hat{\mathbf{I}}_q(t)\,\mathrm{d}t + \mathbf{K}_i\int_0^t\int_o^t \operatorname{sign}\left(\hat{\mathbf{I}}_q(t)\right)\mathrm{d}t\,\mathrm{d}t\right]\end{aligned} \tag{22}$$

and its time derivative $\dot{\hat{\boldsymbol{\Omega}}}_r = \ddot{\mathbf{x}}_s - \ddot{\hat{\mathbf{x}}}_r$ as follows

$$\begin{aligned}\dot{\hat{\boldsymbol{\Omega}}}_r = {} & \ddot{\tilde{\mathbf{x}}}_s + \bar{\mathbf{M}}_s^{-1}[\bar{\mathbf{B}}_s\dot{\tilde{\mathbf{x}}}_s + \mathbf{F}(t)]\\ & + \bar{\mathbf{M}}_s^{-1}\mathbf{K}_i\int_0^t \operatorname{sign}\left(\hat{\mathbf{I}}_q(t)\right)\mathrm{d}t\\ = {} & \bar{\mathbf{M}}_s^{-1}\left[\hat{\mathbf{I}}_q(t) + \mathbf{K}_i\int_0^t \operatorname{sign}\left(\hat{\mathbf{I}}_q(t)\right)\mathrm{d}t\right]\end{aligned} \tag{23}$$

where $\mathbf{K}_i$ is the $n \times n$ sliding mode diagonal definite positive gain matrix and $\operatorname{sign}(\hat{\mathbf{I}}_q) = [\operatorname{sign}(\hat{\mathbf{I}}_{q1}), \ldots, \operatorname{sign}(\hat{\mathbf{I}}_{qn})]$ is the discontinuous signum function of $\hat{\mathbf{I}}_q$.

Subsequently, the control law for the slave is given.

Impedance passive computed torque control

The proposed slave control is expressed in terms of the nominal reference as follows

$$\mathbf{F}_s = \mathbf{H}_s\ddot{\hat{\mathbf{x}}}_r + \mathbf{C}_s\dot{\hat{\mathbf{x}}}_r + \mathbf{G}_s + \mathbf{F}_e - \mathbf{K}_g\hat{\boldsymbol{\Omega}}_r \tag{24}$$

By considering equation (20), the above expression can be rewritten as follows

$$\mathbf{F}_s = \hat{\mathbf{Y}}_r\boldsymbol{\Theta} + \mathbf{F}_e - \mathbf{K}_g\hat{\boldsymbol{\Omega}}_r \tag{25}$$

where $\mathbf{K}_g$ is an $n \times n$ gain matrix. It is worth noticing that equation (25) is a chattering-free controller since $\hat{\boldsymbol{\Omega}}_r$ comprises the integral of the signum function, which is now a continuous function. High-frequency signals are inconceivable in electromechanical systems due to their finite bandwidth; that is why second-order sliding modes are a better choice rather than first-order sliding modes. The term $\mathbf{K}_g\hat{\boldsymbol{\Omega}}_r$ has been added to achieve exponential stability, as it will be seen afterwards. Also, note that equation (17) requires measurement of acceleration because $\hat{\mathbf{I}}_e$ depends on acceleration. To deal with this situation, velocity and acceleration are estimated, on both master and slave sides (see Figure 1 for major reference), by means of the robust *exact differentiator* given in equation (11). In this case position, terminal higher-order sliding modes are used to differentiate l times ($l = 2$), a desired input. Since the estimation error converges to zero in finite time, then there is no need to verify the principle of separation, as it is stated in the literature,[23,26] provided that the differentiator dynamics is faster than the master and slave dynamics.

Remark 3. Since the estimation error converges to zero in finite time, the separation principle is satisfied automatically; thus, closed-loop dynamics given by equation (17) holds.

Remark 4. In the absence of noise and after the observer's finite-time transient, its outputs can be considered as exact measurements of the derivatives. However, in the presence of measurement noises, the differentiation accuracy inevitably deteriorates rapidly with the growth of the differentiation order.[23] In our case, the differentiation order is two, so it is not expected to experience a low accuracy. Even when treating noisy signals, the observer performance only improves with the sampling step reduction. In our case, sampling time is relatively small: 1 ms.

Remark 5. By carefully tuning constants $\lambda_0, \lambda_1, \lambda_2 > 0$ for each observer, a faster dynamics response can be achieved. A tuning procedure is given in the study by Levant.[23]

Stability analysis

In this section, the stability analysis of the closed-loop dynamics of both master and slave systems is studied as well as the whole teleoperation system.

Master stability analysis

Closed-loop system (12) describes a set of n decoupled second-order differential linear equations that exhibit stable behaviour by a suitable choice of the matrices $\bar{\mathbf{M}}_m,\ \bar{\mathbf{B}}_m,\ \bar{\mathbf{K}}_m$.

Slave stability analysis

Theorem 1. Substituting the control law (24) into the slave robot dynamics (4) yields the closed-loop dynamics

$$\mathbf{H}_s\dot{\hat{\mathbf{\Omega}}}_r = -\mathbf{K}_g\hat{\mathbf{\Omega}}_r - \mathbf{C}_s\hat{\mathbf{\Omega}}_r \tag{26}$$

which describes a first-order differential non-linear equation in the new variable $\hat{\mathbf{\Omega}}_r$. Thus local exponential tracking is assured, provided that $\mathbf{K}_i$ and $\mathbf{K}_g$ are large enough, for small initial error conditions.

Proof. Stability analysis is divided into two parts.

Closed-loop signals boundedness. Let us consider the following Lyapunov candidate function

$$V = \frac{1}{2}\hat{\mathbf{\Omega}}_r^T\mathbf{H}_s\hat{\mathbf{\Omega}}_r \tag{27}$$

whose time derivative along the trajectories of the system is as follows

$$\dot{V} = \frac{1}{2}\hat{\mathbf{\Omega}}_r^T\dot{\mathbf{H}}_s\hat{\mathbf{\Omega}}_r + \hat{\mathbf{\Omega}}_r^T\mathbf{H}_s\dot{\hat{\mathbf{\Omega}}}_r \tag{28}$$

Substituting equation (26) into equation (28) results in

$$\begin{aligned}\dot{V} &= \frac{1}{2}\hat{\mathbf{\Omega}}_r^T\dot{\mathbf{H}}_s\hat{\mathbf{\Omega}}_r + \hat{\mathbf{\Omega}}_r^T(-\mathbf{K}_g\hat{\mathbf{\Omega}}_r - \mathbf{C}_s\hat{\mathbf{\Omega}}_r)\\ &= -\hat{\mathbf{\Omega}}_r^T\mathbf{K}_g\hat{\mathbf{\Omega}}_r\end{aligned} \tag{29}$$

where the well-known skew-symmetry property $[\hat{\mathbf{\Omega}}_r^T(\dot{\mathbf{H}}_s - 2\mathbf{C}_s)\hat{\mathbf{\Omega}}_r = 0]$ has been used. From equation (29), it is evident that $\hat{\mathbf{\Omega}}_r$ is bounded and so it is $\dot{\hat{\mathbf{\Omega}}}_r$. Thus, the closed-loop signals are bounded.

Second-order sliding mode condition. Now, to prove the existence of the sliding mode, it is necessary to verify the sliding mode condition $\hat{\mathbf{I}}_q\dot{\hat{\mathbf{I}}}_q \le -\mu|\hat{\mathbf{I}}_q|$. Differentiating twice equation (22) gives rise to

$$\ddot{\hat{\mathbf{\Omega}}}_r = \bar{\mathbf{M}}_s^{-1}\left[\dot{\hat{\mathbf{I}}}_q + \mathbf{K}_i\,\mathrm{sign}(\hat{\mathrm{I}}_q)\right] \tag{30}$$

Multiplying $\ddot{\hat{\mathbf{\Omega}}}_r$ by $\hat{\mathbf{I}}_q^T$, solving for $\hat{\mathbf{I}}_q\dot{\hat{\mathbf{I}}}_q$, and multiplying by $\bar{\mathbf{M}}_s$ give rise to the following

$$\hat{\mathbf{I}}_q\dot{\hat{\mathbf{I}}}_q = \hat{\mathbf{I}}_q^T\bar{\mathbf{M}}_s\ddot{\hat{\mathbf{\Omega}}}_r - \hat{\mathbf{I}}_q\mathbf{K}_i\,\mathrm{sign}(\hat{\mathbf{I}}_q) \tag{31}$$

$$\begin{aligned}\hat{\mathbf{I}}_q\dot{\hat{\mathbf{I}}}_q &= \hat{\mathbf{I}}_q\bar{\mathbf{M}}_s\ddot{\hat{\mathbf{\Omega}}}_r - \mathbf{K}_i|\hat{\mathbf{I}}_q|\\ &\le |\hat{\mathbf{I}}_q||\bar{\mathbf{M}}_s||\ddot{\hat{\mathbf{\Omega}}}_r| - \mathbf{K}_i|\hat{\mathbf{I}}_q|\\ &\le -\Big(\lambda_m(\mathbf{K}_i) - \epsilon\Big)|\hat{\mathbf{I}}_q|\\ &\le -\mu|\hat{\mathbf{I}}_q|\end{aligned} \tag{32}$$

where $\mu = \lambda_m(\mathbf{K}_i) - \epsilon$ and $|\ddot{\hat{\mathbf{\Omega}}}_r| \le \epsilon$, with $\lambda_m(\mathbf{K}_i)$ describing the minimum eigenvalue of $\mathbf{K}_i$. Matrix $\bar{\mathbf{M}}_s$ is bounded since it is given by the user. Thus, the sliding condition is obtained if $\lambda_m(\mathbf{K}_i) > \epsilon$, such that $\mu > 0$ in equation (32) guarantees the sliding mode on $\hat{\mathbf{I}}_q = 0$ at $t_r \le \frac{|\hat{\mathbf{I}}_q(t_0)|}{\mu}$. Note that for any initial condition $\hat{\mathbf{I}}_q(t_0) = 0$, then $t_r = 0$, which implies that the sliding mode condition is enforced for all the time. Therefore, expression (32) leads to equation (17)

$$\mathbf{I}_e = 0 \Rightarrow \bar{\mathbf{M}}_s\ddot{\tilde{\mathbf{x}}}_s + \bar{\mathbf{B}}_s\dot{\tilde{\mathbf{x}}}_s + \bar{\mathbf{K}}_s\tilde{\mathbf{x}}_s + \mathbf{F}_e = 0$$

which means that, asymptotically,

$$\mathbf{I}_e = 0 \Rightarrow \begin{cases} \mathbf{F}_e = 0,\ \mathbf{x}_s \to k_p\mathbf{x}_m^{T_d},\ \dot{\hat{\mathbf{x}}}_s \to k_p\dot{\hat{\mathbf{x}}}_m^{T_d} \\ \ddot{\hat{\mathbf{x}}}_s \to k_p\ddot{\hat{\mathbf{x}}}_m^{T_d} \\ \mathbf{F}_e > 0,\ \text{impedance tracking} \end{cases} \tag{33}$$

where $\mathbf{F}_e = 0$ stands for the free motion regime and $\mathbf{F}_e > 0$ stands for the constrained motion regime.

Stability of the teleoperation system

Last section presented the control law for each station, master and slave, and their individual stability analysis. However, the overall teleoperation stability system must also be addressed.

Passivity is an intuitive tool that examines the energy flows in a system and makes stability assertions if energy is dissipated instead of generated.[27] The proposed teleoperation system includes a human operator, an environment, two manipulators, and the communication channel. Considering that the human operators and the environment are passive,[28] and since the nature of manipulators, the only source of instability of the system is the communication channel.[29] According to the system structure, the communication channel can be analysed as a two-port network, which relates flows and efforts from one side to another and vice versa. The relationship between network flows $\mathbf{Y}(s) = [\dot{\mathbf{x}}_m(s), \dot{\mathbf{x}}_s(s)]^T$ and efforts $\mathbf{U}(s) = [\mathbf{F}_h(s), \mathbf{F}_e(s)]^T$ can be described by means of a hybrid matrix $\mathbf{H}(s)$ for each Cartesian axis. Note that the network output vector $\mathbf{Y}(s)$, the network input vector $\mathbf{U}(s)$, and the matrix $\mathbf{H}(s)$ are the

functions in the complex frequency domain. The matrix is obtained using the impedance models of master and slave, equations (12) and (16), respectively. In the x-axis, the hybrid matrix is expressed as follows

$$\mathbf{Y}_x(s) = \mathbf{H}_x(s)\mathbf{U}_x(s)$$

$$\begin{bmatrix} \mathrm{F}_{hx}(s) \\ \dot{x}_s(s) \end{bmatrix} = \begin{bmatrix} \mathrm{h}_{x11}(s) & \mathrm{h}_{x12}(s) \\ \mathrm{h}_{x21}(s) & \mathrm{h}_{x22}(s) \end{bmatrix} \begin{bmatrix} \dot{x}_m(s) \\ -\mathrm{F}_{ex}(s) \end{bmatrix}$$

where the elements of the hybrid matrix are as follows

$$\mathrm{h}_{x11} = \left[\frac{\mathrm{F}_{hx}(s)}{\dot{x}_m(s)}\right]_{\mathrm{F}_{ex}=0} = \bar{\mathrm{M}}_{m11}s + \bar{\mathrm{B}}_{m11} + \frac{\bar{\mathrm{K}}_{m11}}{s}$$

$$\mathrm{h}_{x12} = \left[\frac{\mathrm{F}_{hx}(s)}{-\mathrm{F}_e(s)}\right]_{\dot{x}_m=0} = -k_f e^{-T_d s}$$

$$\mathrm{h}_{x21} = \left[\frac{\dot{x}_s(s)}{\dot{x}_m(s)}\right]_{\mathrm{F}_{ex}=0} = k_p e^{-T_d s}$$

$$\mathrm{h}_{x22} = \left[\frac{\dot{x}_s(s)}{-\mathrm{F}_{ex}(s)}\right]_{\dot{x}_m=0} = \frac{s}{\bar{\mathrm{M}}_{s11}s^2 + \bar{\mathrm{B}}_{s11}s + \bar{\mathrm{K}}_{s11}}$$

A similar procedure can be carried out to compute the hybrid matrices for the y- and z-axes. In order to analyse the system stability, the passivity theory is applied.

Theorem 2. A linear, time-invariant n-port network possessing a general hybrid matrix, which is analytic in the open Right Half S-plane (RHS), is passive if and only if the general hybrid matrix is positive real.[30]

Definition. An $n \times n$ matrix function $\mathbf{H}(s)$ of the complex variable $s = \sigma + \mathrm{j}\omega$ is said to be a positive-real matrix if it satisfies the following three conditions[30]:

a) $\mathbf{H}(s)$ is analytic in the open RHS.
b) $\bar{\mathbf{H}}(s) = \mathbf{H}(\bar{s})$ for every s in the open RHS, where $\bar{s}$ denotes the complex conjugate of s.
c) Its Hermitian part $\mathbf{H}_h(s)$ is non-negative definite for all s in the open RHS. It means that all of its principal minors are non-negative which can be obtained as follows

$$\mathrm{Re}\ \mathrm{h}_{11} \geq 0,\ \ \mathrm{Re}\ \mathrm{h}_{22} \geq 0,\ \ 4\,\mathrm{Re}\ \mathrm{h}_{11}\,\mathrm{Re}\ \mathrm{h}_{22} \geq |\mathrm{h}_{12} + \bar{\mathrm{h}}_{21}|^2$$

For the given two-port network, conditions (a) and (b) of realness are held immediately because of the structure of the hybrid matrix elements. They are satisfied with positive impedance parameters. The three conditions of (c) can be expressed for each Cartesian axis by

$$\bar{\mathrm{B}}_m \geq 0 \tag{34}$$

$$\frac{\bar{\mathrm{B}}_s\omega^2}{(\bar{\mathrm{K}}_s - \bar{\mathrm{M}}_s\omega^2)^2 + (\bar{\mathrm{B}}_s\omega)^2} \geq 0 \tag{35}$$

$$\frac{4\,\bar{\mathrm{B}}_m\,\bar{\mathrm{B}}_s\omega^2}{(\bar{\mathrm{K}}_s - \bar{\mathrm{M}}_s\omega^2)^2 + (\bar{\mathrm{B}}_s\omega)^2} - k_f^2 - k_p^2 + 2k_f k_p \cos(2T_d\omega) \geq 0 \tag{36}$$

The first inequality is satisfied by choosing a positive $\bar{\mathrm{B}}_m$ parameter. The last of condition (c) is satisfied only if

$$\frac{4\,\bar{\mathrm{B}}_m\,\bar{\mathrm{B}}_s\omega^2}{(\bar{\mathrm{K}}_s - \bar{\mathrm{M}}_s\omega^2)^2 + (\bar{\mathrm{B}}_s\omega)^2} \geq (k_f + k_p)^2,\ \forall\omega \geq 0 \tag{37}$$

If the design parameters satisfy equations (35) and (37), the teleoperation system will be passive for any set of passive human operators and environments even with the presence of constant time delay.[15,30]

Remark 6. Master controller tuning.
Master impedance parameters are tuned, such that a comfortable operation can be achieved. A higher impedance yields a heavier and more sluggish performance, while a lower impedance makes the master teleoperator weightless and, in general, more difficult to drive, depends on operator's dexterity. Then tuning of the controller is made heuristically, provided that the choosing of $\bar{\mathrm{B}}_m$ contributes to the slave's stability, according to equations (34)–(36).

Remark 7. Slave controller tuning.
First of all, impedance parameters must be chosen, such that equations (34)–(36) are fulfilled. Similar to the master controller tuning, slave impedance tuning is made heuristically, provided that a wide range of frequencies are allowed when evaluating equations (34)–(36). Additional stability and improvement of the performance, as the stability proof suggests, is to set an arbitrary $\mathbf{K}_g > 0$, such that error dynamics remains bounded. Increase $\mathbf{K}_g$ until acceptable boundedness of $\hat{\mathbf{\Omega}}$ is achieved. Then, increase gradually $\mathbf{K}_i$ until the sliding mode arises ($\hat{\mathbf{I}}_q = 0$). Finally, a faster and better tracking position can be accomplished by increasing $\mathbf{K}_g$ and $\bar{\mathbf{K}}_s$, respectively.

Experimental results

Semi-experimental set-up

In this section, the performance of the proposed control scheme is evaluated by means of experimentation carried out in a semi-experimental set-up. The semi-experimental set-up (shown in Figure 2) is fitted with a Phantom Premium 1.0 haptic interface (used as the master robot) and a NANO17 six-DOF force/torque sensor attached to the Phantom's end effector to measure the human operator input force. The complete system, haptic interface and virtual environment run in a personal computer under Windows XP operating system. The virtual slave robot mimics the industrial robot Catalyst-5, and its dynamics is solved online by a well-known numerical integrator. The communication channel is emulated with an First-In First-Out (FIFO) memory buffer that introduces bilateral time delays. The data to be exchanged between the master and the slave are stored in the buffer instead of sending them immediately to their destination. The data are released only at the moment when the buffer is full. Thus, the magnitude of the

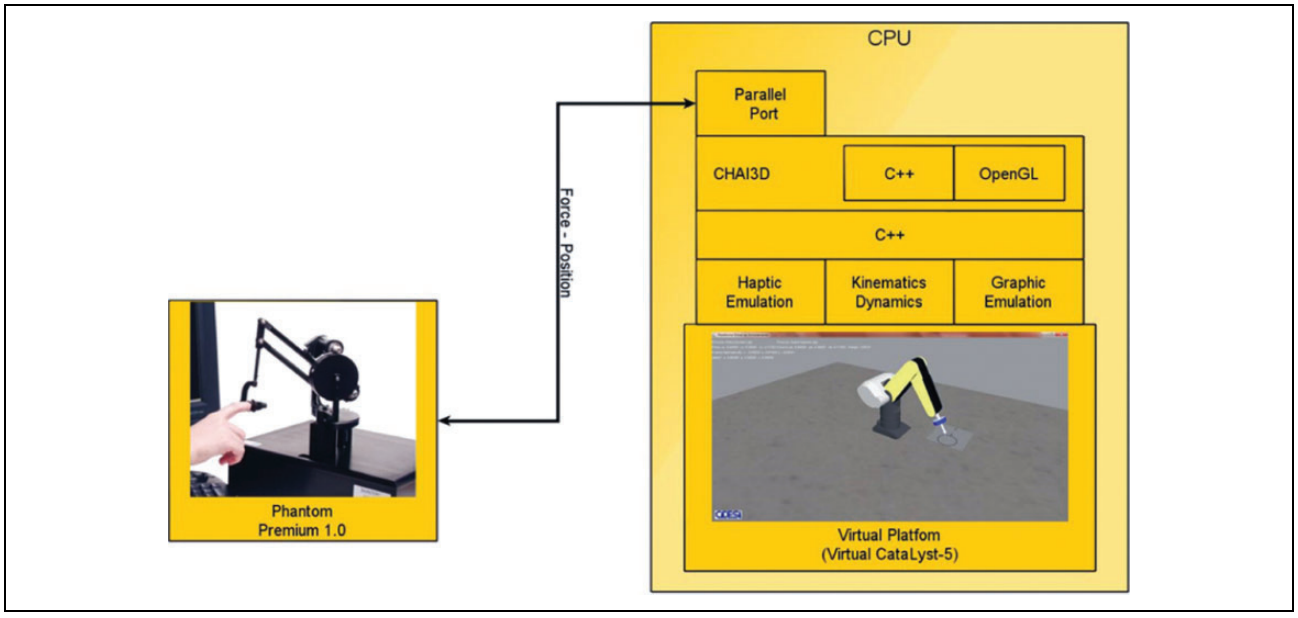

Figure 2. Semi-experimental set-up.

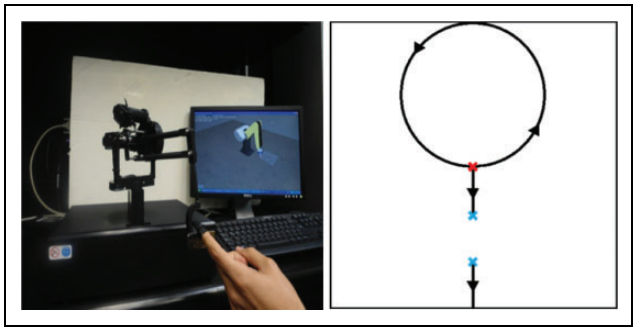

Figure 3. Definition of the task: standard trajectory to be followed by the operator.

time delay depends on the size of the buffer. The combination of Visual C++, CHAI3D and OpenGL libraries allows the user to interact with a high fidelity and realistic virtual environment in real time.

Robot and controllers parameters

The slave robot (virtual robot) is teleoperated in such a way that its end effector follows a predefined trajectory, as it is shown in Figure 3. The sequence is as follows. The master and the slave robot's initial conditions are different and isolated from the virtual plane. The operator approaches to the plane to make contact at the red point, as shown in Figure 3 (right). Then, the operator requests the slave robot's end effector to follow the circumference while exerting a sustained level of force onto the plane. After the completion of one circumference, the operator follows a segment of straight line, stops exerting force and again starts exerting a sustained force onto the plane while moving along the last straight line segment. The experiments last approximately 17 s.

Table 1. Master controller feedback gains.

Gain	Value
$\bar{\mathbf{M}}_m$	diag(0.01)
$\bar{\mathbf{B}}_m$	diag(1)
$\bar{\mathbf{K}}_m$	diag(0)

Table 2. Slave controller feedback gains.

Gain	Value
$\bar{\mathbf{M}}_s$	diag(10)
$\bar{\mathbf{B}}_s$	diag(500, 150, 180)
$\bar{\mathbf{K}}_s$.	diag(300, 300, 300)
$\mathbf{K}_g$	diag(7, 1, 5)
$\mathbf{K}_i$	diag(10, 10.5, 10.7)
κ	6

To perform the above desired task, feedback gains for the master and slave controllers are given in Tables 1 and 2.

Scaling factors are set as follows: $k_p = 2.7$ and $k_f = 1.0$. Differentiator parameters are set as follows: $\lambda_{0j} = 45$, $\lambda_{1j} = 35$ and $\lambda_{2j} = 120$, where $j = x, y, z$.

Environment parameters. The virtual plane (environment) is modelled as a spring whose stiffness coefficient $K_{ez} = 360\ N/m$. The virtual plane is located at $z_e = 0.1\ m$ in z-axis and is parallel to the x-y plane on the slave robot's base frame; thus, the environment force is $F_e = K_{ez}\Delta \mathrm{z}$, with $\Delta \mathrm{z} = \mathrm{z} - z_e$ as the deformation of the virtual plane (see Figure 4 for reference).

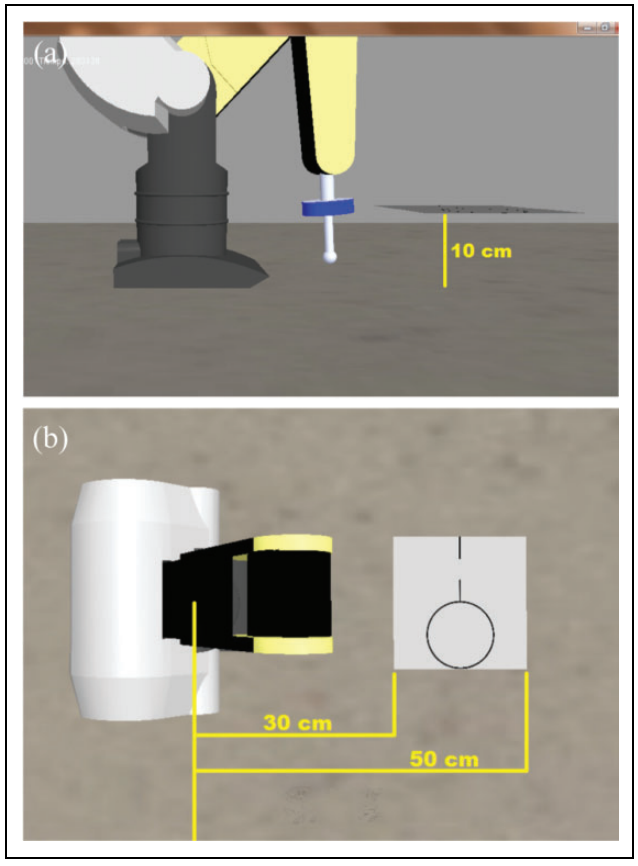

Figure 4. Location of the virtual plane with respect to the slave robot base frame.

Slave robot parameters. Parameters are those of the Catalyst-5 industrial robot. Only the first three DOFs are modelled and controlled; pitch and roll joints are fixed. Table 3 lists the main robot parameters.

Results

Two sets of experiments were carried out. The first set does not consider time delay, that is, $T_d = 0\,\text{s}$ (see equations (6) and (7) for detail). The second set does consider a constant time delay $T_d = 1\,\text{s}$. So the roundtrip time delay is 2 s.

Figures 5 to 8 depict the experimental results considering a time delay $T_d = 0\,\text{s}$. Figure 5 shows master and slave Cartesian trajectories in three-dimensional view. Note that the slave Cartesian trajectory is greater than the master trajectory; this is because of the scaling factor $k_p = 2.7$.

Figure 6 shows the position tracking for each joint. Note that the position tracking error is very close to zero, as it can be seen in Figure 7. Finally, Figure 8 shows that the human force and the environment force are very similar; an issue that suggests a good level of transparency.

Figures 9 to 12 depict the experimental results considering a time delay $T_d = 1\,\text{s}$. Note that in this case, due to time delay, the task is performed in a longer time; mainly because the slave interacts with the environment. The master and slave trajectories in the Cartesian space can be seen from Figure 9. Figures 10 and 11 exhibit a good tracking performance as it stated by equation (33). Finally, Figure 12 depicts the human force and the environment force when the slave interacts with the environment. According to the task that the human operator has to carry out (see Figure 3

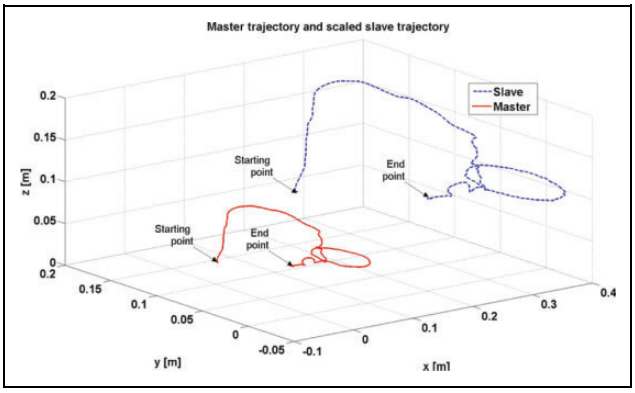

Figure 5. Three-dimensional view of Cartesian master and slave trajectories ($T_d = 0\,\text{s}$).

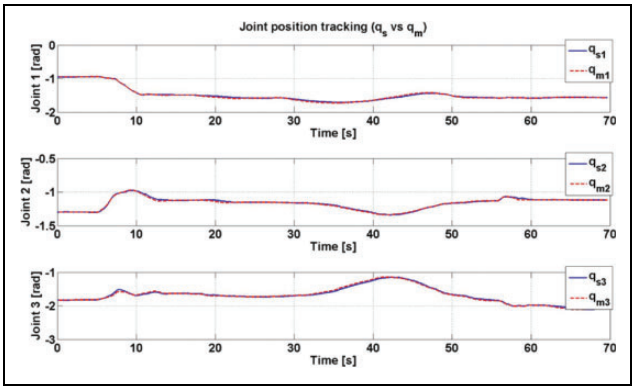

Figure 6. Joint position tracking on the slave side ($T_d = 0\,\text{s}$).

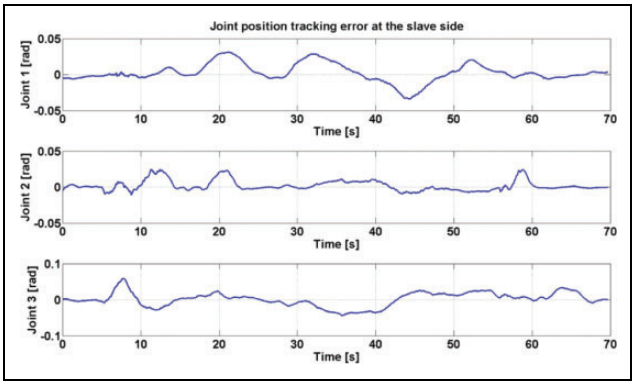

Figure 7. Joint position tracking error on the slave side ($T_d = 0\,\text{s}$).

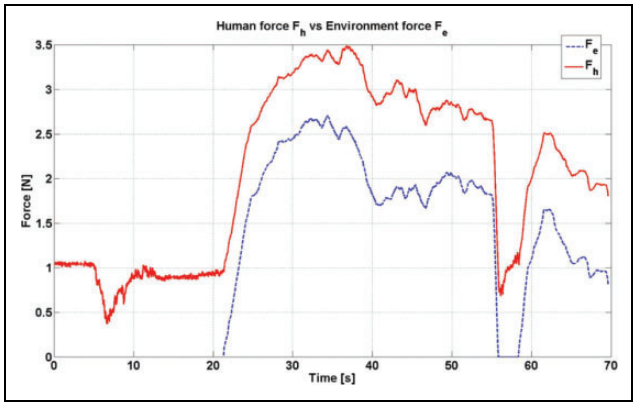

Figure 8. Human force versus environment force ($T_d = 0$ s)

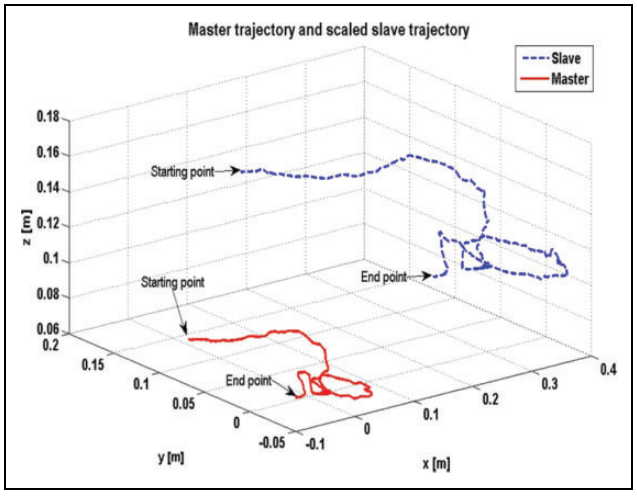

Figure 9. Three-dimensional view of Cartesian master and slave trajectories ($T_d = 1$ s).

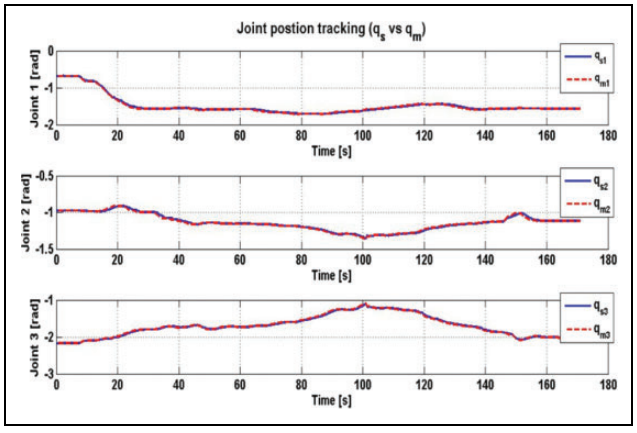

Figure 10. Joint position tracking on the slave side ($T_d = 1$ s).

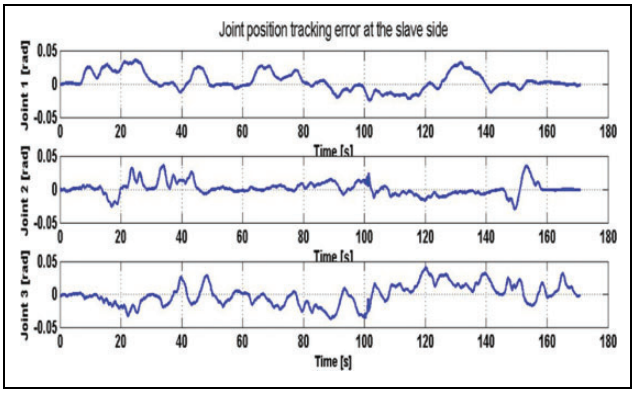

Figure 11. Joint position tracking error at the slave side ($T_d = 1$ s).

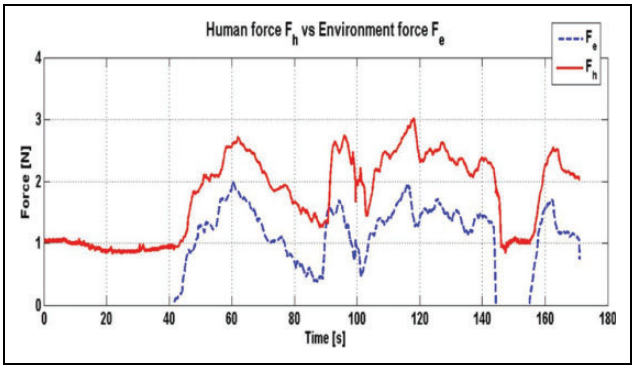

Figure 12. Human force versus environment force ($T_d = 1$ s)

Table 3. Main parameters of the slave robot (Thermo Fisher Scientific Inc.).

Link	Mass	Length
Link 1	9.0	0.2504
Link 2	2.0	0.2504
Link 3	1.0	0.25.4
Units	kg	m

for reference), note that exerting a sustained force onto the plane becomes very difficult due to the time delay. The latter is evident during the course of the circumference (performed in about 115 s, from 40 s to 155 s, approximately). Similar to the first set of experiments ($T_d = 0$ s), human force and environment force are very similar, which suggests a good kinesthetic coupling.

Conclusions

In this article, a robust but smooth bilateral teleoperation scheme that achieves exponential tracking performance under unknown constant time delay is proposed. Formal analysis of stability for the whole teleoperation system demonstrates passivity for multi-DOF non-linear teleoperators. Experimental results reveal the effectiveness of the approach.

Several factors are involved here to guarantee the stability of the whole teleoperation system (human operator + master robot + communication channel + slave robot + environment). On one hand, master controller and slave

controller have been designed separately (independently of time delay), that is, locally, each controller guarantees stability. On the other hand, it is well known that the communication channel is the main source of instability when time delay is present. Therefore, in order to prove the stability of the entire teleoperation system, considering time delay induced by the communication channel, the *n*-port network theory (originally developed for electrical systems) was taken into account. Thus, analysing the master robot + communication channel + slave robot system (assuming that human operator and environment are passive) as a two-port network, it can be concluded passivity, regarding unknown constant time delay. Finally, but not least important, it is documented in several works that second-order sliding mode control (at the slave side) provides with additional robustness against time delay and parametric uncertainty.

Future work is to design an adaptive control based on the new nominal reference proposed in this article and evaluate its performance.

Declaration of conflicting interests

The author(s) declared no potential conflicts of interest with respect to the research, authorship, and/or publication of this article.

Funding

The author(s) disclosed receipt of the following financial support for the research, authorship and/or publication of this article: Garcia-Valdovinos and Bandala-Sánchez acknowledge support from SEP-CONACYT projects 61499 and 239089, respectively. The other authors thank CONACYT scholarship support.

References

1. Sarras I, Nuño E, Kinnaert M, et al. Output-feedback control of nonlinear bilateral teleoperators. In: *2012 American control conference*, Montreal, Canada, 27–29 June 2012.
2. Chopra N, Spong M, Ortega R, et al. On tracking performance in bilateral teleoperation. *IEEE Trans Robot* 2006; 22(4): 861–866.
3. Ryu J-H, Artigas J and Preusche P. A passive bilateral control scheme for a teleoperator with time-varying communication delay. *Mechatronics* 2010; 20: 812–823.
4. Lee D and Spong M. Passive bilateral teleoperation with constant time delay. *IEEE Trans Robot* 2006; 22(2): 9–281.
5. Hokayem P and Spong M. Bilateral teleoperation: an historical survey. *Automatica* 2006; 42(12): 2035–2057.
6. Lichiardopol S. *A survey on teleoperation*. Eindhoven: Technische Universiteit Eindhoven, 2007.
7. RodrIguez-Seda E, Lee D and Spong W. Experimental comparison study of control architectures for bilateral teleoperators. *IEEE Trans Robot* 2009; 25(6): 1304–1318.
8. Nuño E, Basañez L and Ortega R. Passivity-based control for bilateral teleoperation: a tutorial. *Automatica* 2011; 47: 485–495.
9. Garcia-Valdovinos L, Parra-Vega V and Arteaga M. Robust bilateral teleoperation control under unknown constant time delay without velocity measurements: *SYROCO*, Bologna, Italy, 6–8 September 2006.
10. Garcia-Valdovinos L, Parra-Vega V and Arteaga M. Observer-based sliding mode impedance control of bilateral teleoperation under constant time delay. *Robot Auton Syst* 2007; 55: 609–617.
11. Ghafarirad H, Rezaei S, Abdullah A, et al. Observer-based sliding mode control with adaptive perturbation estimation for micropositioning actuators. *Precis Eng* 2011; 35(2): 271–281.
12. Gonzalez N, de León J, Guerra C, et al. A sliding mode-based impedance control for bilateral teleoperation under time delay. In: *18th IFAC world congress*, Milan, Italy, 28 August–2 September 2011.
13. Buttolo P, Braathen P and Hannaford B. Sliding control of force reflecting teleoperation: preliminary studies. *Presence* 1994; 3(2): 158–172.
14. Park JH and Cho C. Sliding mode controller for bilateral teleoperation with varying time delay. In: *EEE international conference on advanced intelligent mechatronics*, Atlanta, USA, 19–23 September 1999.
15. Cho H, Park JH, Kim K, et al. Sliding mode based impedance controller for bilateral teleoperation under varying time delay. In: *IEEE international conference on robotics and automation*, Seoul, Korea, 21–26 May 2001, pp. 1025–1030.
16. Cho H and Park JH. Stable bilateral teleoperation under a time delay using a robust impedance control. *Mechatronics*, 2005; 15(5): 611–625.
17. Shahbazi M, Talebi H and Yazdanpanah M. A control architecture for dual user teleoperation with unknown time delays: a sliding mode approach. In: *IEEE/ASME international conference on advanced intelligent mechatronics*, Montréal, Canada, 6–9 July 2010.
18. Ghafarirad H, Rezaei SM, Zareinejad M, et al. A robust adaptive control for micro-positioning of piezoelectric actuators with environment force estimation. *Transactions of the Institute of Measurement and Control* 2011; 0(0): 1–10.
19. Hace A and Franc M. FPGA implementation of sliding-mode-control algorithm for scaled bilateral teleoperation. *IEEE Trans Ind Inform* 2013; 9(3): 1291–1300.
20. Vafaei A and Yazdanpanah M. Terminal sliding mode impedance control for bilateral teleoperation under unknown constant time delay and uncertainties. In: *European control conference*, Zurich, Switzerland, 17–19 July 2013.
21. Garcia-Valdovinos L, Parra-Vega V and Arteaga M. Higher-order sliding mode impedance bilateral teleoperation with robust state estimation under constant unknown time delay. In: *IEEE/ASME international conference on advanced intelligent mechatronics*, Monterey, CA, 24–28 July 2005.
22. Olguin-Diaz E, Parra-Vega V, Garcia-Valdovinos L, et al. Design parametrization for dynamically similar delayed teleoperation systems. In: Cetto JA, Filipe J and Ferrier J-L (eds) *Informatics in control automation and robotics*. Berlin: Springer-Verlag, 2011, pp. 143–155.

23. Levant A. Higher-order sliding modes, differentiation and output-feedback control. *Int J Control* 2003; 76(9–10): 924–941.
24. Hogan N. Impedance control: an approach to manipulation: part I - theory. *J Dyn Syst Meas Control* 1985; 107(1): 1–7.
25. Kelly R, Santibañez V and Loria A. *Control of robot manipulators in joint space*. Berlin Heidelberg: Springer-Verlag, 2005.
26. Davila J, Fridman L and Levant A. Second-order sliding-mode observer for mechanical systems. *IEEE Trans Autom Control* 2005; 50(11): 1785–1789.
27. Niemeyer G, Preusche C and Hirzinger G. Telerobotics. In: Siciliano D and Khatib O (eds) *Handbook of robotics*. Berlin-Heilderberg: Springer, 2008, pp. 741–757.
28. Weir D and Colgate J. Stability of haptic displays. In: Lin MC and Otaduy M (eds) *Haptic rendering: foundations, algorithms, and applications*. Wellesley: AK Peters/CRC Press, 2008, pp. 151–189.
29. Anderson R and Spong M. Bilateral control of teleoperators with time delay. *IEEE Trans Autom Control* 1989; 34(5): 494–501.
30. Chen W-K. *Active network analysis*. River Edge: World Scientific Publishing Co., 1991.